

RESEARCH

Open Access



# Bifurcation analysis of a discrete *SIRS* epidemic model with standard incidence rate

Zengyun Hu<sup>1,2</sup>, Linlin Chang<sup>3</sup>, Zhidong Teng<sup>3</sup> and Xi Chen<sup>1\*</sup>

\*Correspondence:

chenxi@ms.xjb.ac.cn

<sup>1</sup>State Key Laboratory of Desert and Oasis Ecology, Xinjiang Institute of Ecology and Geography, Chinese Academy of Sciences, Urumqi, 830011, People's Republic of China  
Full list of author information is available at the end of the article

## Abstract

Discrete epidemic models are popularly used to detect the pathogenesis, spreading, and controlling of the diseases. The three-dimensional discrete *SIRS* epidemic models are more suitable than the two-dimensional discrete models to describe the spreading characters of the diseases. In this paper, the complex dynamical behaviors of a three-dimensional discrete *SIRS* epidemic model with standard incidence rate are discussed. We choose the time step size parameter as a bifurcation parameter, the existence, stability, and direction of Hopf bifurcation are proved by using the normal form theorem and bifurcation theory. Moreover, the numerical simulations not only illustrate our results, but they also exhibit the complex dynamical behaviors, such as the invariant cycle, period-7 orbits and period-12 orbits with more than one attractors and chaotic sets. The flip bifurcation caused by the step size parameter is also obtained by a numerical simulation. Most importantly, when the adequate contact rate and the death rate of the infective individuals are chosen as the bifurcation parameters, there also exist a Hopf bifurcation, a flip bifurcation, chaos, and strange attractors. These results provide significant information for the disease controlling when there appear complex dynamical behaviors in the epidemic model.

**MSC:** 37L15; 37L10; 39A10

**Keywords:** discrete *SIRS* model; flip bifurcation; Hopf bifurcation; chaos; complex dynamical behavior

## 1 Introduction

As is well known, in the study of epidemic theory, mathematical models have been widely used to detect the stability, periodicity, extinction, permanence, bifurcations, and more complex dynamical behaviors of the diseases (see, for example, [1–20] and the references cited therein). There are two kinds of mathematical models to detect the dynamical behaviors of the diseases: the continuous-time models described by differential equations and the discrete-time models described by difference equations. Recently, discrete-time epidemic models have received more and more attention (see, for example, [11–33] and the references cited therein). The detailed reasons can be found in [33].

Usually, in the study of disease spreading, the population is classified into three types of individuals: susceptible individuals (*S*), infective individuals (*I*), and recovered individuals (*R*). The basic epidemic models are as follows: *SI* models (the disease is difficult to cure); *SIS* models (the disease can be cured); *SIR* models (the disease is cured with lifelong immunity), and *SIRS* models (the disease is cured with temporary immunity). However,

lots of diseases have temporary immunity, such as influenza, pertussis, gonorrhoea, and so on. Therefore, the *SIRS* epidemic models are important and significant for detecting the pathogenesis, spreading, and controlling of the epidemics.

The following continuous-time *SIRS* epidemic model with standard incidence rate is considered:

$$\begin{aligned} \dot{S}(t) &= A - d_1 S - \lambda \frac{SI}{S + I + R} + \sigma R, \\ \dot{I}(t) &= \lambda \frac{SI}{S + I + R} - (d_2 + \gamma)I, \\ \dot{R}(t) &= \gamma I - (d_3 + \sigma)R, \end{aligned} \tag{1}$$

which has been studied in [34], where  $S(t)$ ,  $I(t)$ , and  $R(t)$  denote the numbers of susceptible, infective, and recovered individuals at time  $t$ , respectively.  $A$  is the recruitment rate of the population,  $d_i$  ( $i = 1, 2, 3$ ) is the death rate of  $S(t)$ ,  $I(t)$ , and  $R(t)$ , respectively.  $\lambda$  is the adequate contact rate,  $\gamma$  is the recovery rate of the infective individuals,  $\sigma$  is the rate by which the recovered individuals become susceptible again. For the model (1), the authors showed that when the basic reproduction number  $\mathfrak{R}_0 = \frac{\lambda}{d_2 + \gamma} < 1$ , then the disease-free equilibrium  $E_0$  is a globally asymptotically stable, endemic equilibrium and  $E^*$  does not exist; and when the basic reproduction number  $\mathfrak{R}_0 > 1$ , then the disease-free equilibrium  $E_0$  is unstable, and the endemic equilibrium  $E^*$  is locally asymptotically stable [34].

In [33], by using the forward Euler scheme we discretized model (1) into the following *SIRS* epidemic model with standard incidence rate:

$$\begin{cases} S_{n+1} = S_n + h[A - d_1 S_n - \lambda \frac{S_n I_n}{S_n + I_n + R_n} + \sigma R_n], \\ I_{n+1} = I_n + h[\lambda \frac{S_n I_n}{S_n + I_n + R_n} - (d_2 + \gamma)I_n], \\ R_{n+1} = R_n + h[\gamma I_n - (d_3 + \sigma)R_n], \end{cases} \tag{2}$$

where parameters  $A$ ,  $d_i$  ( $i = 1, 2, 3$ ),  $\lambda$ ,  $\sigma$ , and  $\gamma$  are given as in model (1), and  $h$  is the time step size.

From the above process of discretization, we can imagine that, when the time step size  $h$  is small enough, the properties of the stability of model (2) should be the same as that of model (1). There will appear an important and interesting problem for model (2): whether there exists a critical value  $h^*$ , such that when  $0 < h < h^*$ , if the basic reproduction number  $\mathfrak{R}_0 = \frac{\lambda}{d_2 + \gamma} < 1$ , then the disease-free equilibrium  $E_0$  is globally asymptotically stable. And if  $\mathfrak{R}_0 > 1$ , then  $E_0$  is unstable, while the endemic equilibrium  $E^*$  exists and is locally asymptotically stable.

The local stability of the disease-free equilibrium and endemic equilibrium for discrete-time *SIRS* epidemic models with general nonlinear incidence rates was first studied in [33]. As an application of the main results, in [33] for model (2) the authors showed that there is a constant  $h^* > 0$  such that when  $h \in (0, h^*)$  if the basic reproduction number  $\mathfrak{R}_0 = \frac{\lambda}{d_2 + \gamma} < 1$ , then the disease-free equilibrium  $E_0$  is locally asymptotically stable, and if  $\mathfrak{R}_0 > 1$ , then the disease-free equilibrium  $E_0$  is unstable, the endemic equilibrium  $E^*$  is locally asymptotically stable (see Corollary 2 in [33]). Further, the numerical simulations in [33] show that when  $\mathfrak{R}_0 > 1$  and  $h > h^*$ , the dynamical behavior of discrete-time model (2) is more complex than the corresponding continuous-time model (1). Moreover, the permanence and extinction of the disease for model (2) are obtained in [35].

However, the study of the complex dynamical behaviors of model (2), especially the Hopf bifurcation, also is very important for the transmission and controlling of the disease. We note that the investigations on the complex dynamical behaviors of model (2) are still unclear. In particular, the studies on the existence, stability, and direction of the Hopf bifurcation are only based on numerical simulations.

Therefore, in this study, the time step size  $h$  is chosen as a bifurcation parameter to study the existence of Hopf bifurcation for model (2) by using the normal form method and the bifurcation theory. Finally, we present numerical simulations to illustrate our results, and actualize the Hopf bifurcation and complex dynamical behaviors of model (2). Most importantly, the adequate contact rate  $\lambda$  and the death rate  $d_2$  of the infective individuals are chosen as the bifurcation parameters and the numerical simulations give the Hopf bifurcation, flip bifurcation, chaos, and strange attractors for model (2).

The organization of this paper is as follows. In Section 2, as preliminaries, we introduce the results obtained in [33] on the existence and local stability of equilibria of model (2). In Section 3, the existence and direction of a Hopf bifurcation of model (2) are discussed. Section 4 presents the numerical simulations, which not only illustrate the theoretical results but also exhibit the complex dynamical behaviors such as the invariant cycle, more than one strange attractors, and chaotic sets. Finally, in Section 5 we give a discussion.

## 2 Local stability of equilibria

The basic reproductive rate for model (2) is  $\mathfrak{R}_0 = \frac{\lambda}{d_2 + \gamma}$ , which denotes the average number of secondary infections generated by an initial population of infected individuals over their lifetimes. Now, on the existence of the nonnegative equilibria of model (2), in [33] we have established the following result.

### Theorem 1

- (1) Model (2) always has a disease-free equilibrium  $E_0(\frac{A}{d_1}, 0, 0)$ .
- (2) If the basic reproductive rate  $\mathfrak{R}_0 > 1$ , then model (2) also has an endemic equilibrium  $E^*(S^*, I^*, R^*)$ , where

$$\begin{cases} S^* = \frac{(d_2 + r)(\gamma + d_3 + \sigma)}{(d_3 + \sigma)(\lambda - d_2 - \gamma)} I^*, \\ R^* = \frac{\gamma}{d_3 + \sigma} I^*, \\ I^* = \frac{(d_3 + \sigma)(\lambda - d_2 - \gamma)}{d_1(d_2 + \gamma)(\gamma + d_3 + \sigma) + (\lambda - d_2 - \gamma)(d_2 d_3 + d_2 \sigma + d_3 \gamma)}. \end{cases}$$

Obviously, model (2) is a special model in [33] when the disease incidence rate  $g(S, I, R) = \lambda \frac{SI}{S+I+R}$ . Then the results about the local stability of disease-free equilibrium  $E_0(\frac{A}{d_1}, 0, 0)$  and the endemic equilibrium  $E^*(S^*, I^*, R^*)$  are the same as in Theorems 2 and 3 in [33], respectively. We omit them in this study, avoiding a repetition.

For detecting the bifurcation of model (2), we know that when the disease-free equilibrium  $E_0(\frac{A}{d_1}, 0, 0)$  and the endemic equilibrium  $E^*(S^*, I^*, R^*)$  are non-hyperbolic, there will exist bifurcation and complex dynamical behaviors for the two equilibria, respectively. In Section 3, we choose the time step size  $h$  as a bifurcation parameter to detect the existence, stability, and bifurcation direction for the Hopf bifurcation by the normal form theorem and bifurcation theory. In Section 4, the numerical simulations are discussed to illustrate our results about the bifurcation and complex dynamical behaviors.

### 3 Analysis of Hopf bifurcation

In this section, for a function  $f(x_1, x_2, \dots, x_n)$ , we denote by  $f_{x_i}$ ,  $f_{x_i x_j}$  and  $f_{x_i x_j x_k}$  the first order partial derivative, the second order partial derivative, and the third order partial derivative of  $f(x_1, x_2, \dots, x_n)$  with respect to  $x_i$ ,  $x_j$ , and  $x_k$ , respectively.

For the endemic equilibrium  $E^*(S^*, I^*, R^*)$ , the corresponding characteristic equation of the Jacobian matrix  $J(E^*)$  can be written as

$$F(w) = w^3 + b_1(h)w^2 + b_2(h)w + b_3(h) = 0, \tag{3}$$

where

$$\begin{aligned} b_1(h) &= -3 - h(a_2 - a_1 - \gamma - \sigma - d_1 - d_2 - d_3), \\ b_2(h) &= 3 + 2h(a_2 - \gamma - \sigma - d_2 - d_3 - a_1 - d_1) + h^2[(a_1 a_2 + a_3 \gamma) \\ &\quad - (\sigma + d_3)(a_2 - \gamma - d_2) - (a_1 + d_1)(a_2 - \gamma - \sigma - d_2 - d_3)], \\ b_3(h) &= -1 + h(a_1 + \gamma + d_1 + d_2 + d_3 + \sigma - a_2) \\ &\quad + h^2[-a_3 \gamma - a_1 a_2 + (d_3 + \sigma)(a_2 - \gamma - d_2) \\ &\quad + (a_1 + d_1)(a_2 - \gamma - \sigma - d_2 - d_3)] \\ &\quad + h^3[a_3 \gamma (a_1 + d_1) - (a_1 + d_1)(d_3 + \sigma)(a_2 - \gamma - d_2) \\ &\quad + a_1 a_2 (d_3 + \sigma) - a_1 \gamma (a_3 + \sigma)], \end{aligned}$$

and

$$a_1 = \frac{\lambda I^*(I^* + R^*)}{(S^* + I^* + R^*)^2}, \quad a_2 = \frac{\lambda S^*(S^* + R^*)}{(S^* + I^* + R^*)^2}, \quad a_3 = \frac{\lambda S^* I^*}{(S^* + I^* + R^*)^2}.$$

Let

$$\bar{A} = b_1^2 - 3b_2, \quad \bar{B} = b_1 b_2 - 9b_3, \quad \bar{C} = b_2^2 - 3b_1 b_3,$$

and

$$\Delta = \bar{B}^2 - 4\bar{A}\bar{C}.$$

We choose the parameters  $A, d_1, \lambda, \sigma, d_2, \gamma, d_3, h$  satisfying  $\Delta > 0$  and the conjugate complex roots  $w_{2,3}$  with the modules equal to one, that is, the case (I) in condition (4) of Theorem 3 in [33]. Then there appears a Hopf bifurcation from the endemic equilibrium  $E^*(S^*, I^*, R^*)$  of model (2).

Now, the existence, stability, and bifurcation direction of the Hopf bifurcation are detected by the normal form theorem and bifurcation theory. First of all, the existence of a Hopf bifurcation is computed by bifurcation theory. The step size  $h$  is chosen as the bifurcation value, which is denoted by  $h^*$ . Giving  $h^*$  a perturbation  $h^{**}$ , model (2) is described by

$$\begin{cases} S_{n+1} = S_n + (h^* + h^{**})[A - d_1 S_n - \lambda \frac{S_n I_n}{S_n + I_n + R_n} + \sigma R_n], \\ I_{n+1} = I_n + (h^* + h^{**})[\lambda \frac{S_n I_n}{S_n + I_n + R_n} - (d_2 + \gamma) I_n], \\ R_{n+1} = R_n + (h^* + h^{**})[\gamma I_n - (d_3 + \sigma) R_n]. \end{cases} \tag{4}$$

Let  $U(n) = S_n - S^*$ ,  $V(n) = I_n - I^*$ , and  $P(n) = R_n - R^*$  in model (4); then we transform the endemic equilibrium  $E^*(S^*, I^*, R^*)$  into the origin, and we have

$$\begin{cases} U(n+1) = U(n) + (h^* + h^{**})[A - d_1(U(n) + S^*) \\ \quad - \lambda \frac{(U(n)+S^*)(V(n)+I^*)}{U(n)+V(n)+P(n)+N^*} + \sigma(P(n) + R^*)], \\ V(n+1) = V(n) + (h^* + h^{**})[\lambda \frac{(U(n)+S^*)(V(n)+I^*)}{U(n)+V(n)+P(n)+N^*} \\ \quad - (d_2 + \gamma)(V(n) + I^*)], \\ P(n+1) = P(n) + (h^* + h^{**})[\gamma V(n) - (d_3 + \sigma)P(n)], \end{cases} \tag{5}$$

where  $N^* = S^* + I^* + R^*$ . The characteristic equation associated with the linearization system of model (4) at  $(0, 0, 0)$  is given by

$$w^3 + b_1(h^*, h^{**})w^2 + b_2(h^*, h^{**})w + b_3(h^*, h^{**}) = 0, \tag{6}$$

where  $b_i(h^*, h^{**})$ ,  $i = 1, 2, 3$ , with the same form as in equation (3).

According to the well-known Cardano formula, equation (5) has one real root,

$$w_1 = -\frac{b_1(h^*, h^{**})}{3} + \left(-\frac{q}{2} + \sqrt{D}\right)^{\frac{1}{3}} - \left(\frac{q}{2} + \sqrt{D}\right)^{\frac{1}{3}},$$

and a pair of conjugate complex roots  $w_{2,3} = \alpha \pm \beta i$ , where

$$\begin{aligned} \alpha &= -\frac{b_1(h^*, h^{**})}{3} - \frac{1}{2} \left[ \left(-\frac{q}{2} + \sqrt{D}\right)^{\frac{1}{3}} - \left(\frac{q}{2} + \sqrt{D}\right)^{\frac{1}{3}} \right], \\ \beta &= \frac{\sqrt{3}}{2} \left[ \left(-\frac{q}{2} + \sqrt{D}\right)^{\frac{1}{3}} - \left(\frac{q}{2} + \sqrt{D}\right)^{\frac{1}{3}} \right], \\ D &= \left(\frac{q}{2}\right)^2 + \left(\frac{p}{3}\right)^3, \\ p &= \frac{3b_2(h^*, h^{**}) - b_1(h^*, h^{**})^2}{3}, \\ q &= \frac{27b_3(h^*, h^{**}) - 9b_1(h^*, h^{**})b_2(h^*, h^{**}) + 3b_1(h^*, h^{**})^3}{27}. \end{aligned}$$

Further, we need

$$k = \frac{d|w_{2,3}|}{dh^{**}} \Big|_{h^{**}=0} \neq 0. \tag{7}$$

Moreover, it is required that, when  $h^{**} = 0$ ,  $w_{2,3}^m \neq 1$ ,  $m = 1, 2, 3, 4$ , which is equivalent to

$$\alpha \neq -\frac{1}{2}, \quad \beta \neq \pm \frac{\sqrt{3}}{2}, \quad (\alpha^2 - \beta^2)^2 - 2\alpha\beta \neq 1. \tag{8}$$

Hence, the eigenvalues  $w_{2,3}$  do not lie in the intersection of the unit circle with the coordinate axes when  $h^{**} = 0$ , and conditions (7) and (8) hold.

In the following, we study the normal form of model (5). Expanding model (5) as a Taylor series at  $(U(n), V(n), P(n)) = (0, 0, 0)$  to the third order, it becomes

$$\begin{cases} U(n+1) = a_{11}U(n) + a_{12}V(n) + a_{13}P(n) + F^*(U(n), V(n), P(n)), \\ V(n+1) = a_{21}U(n) + a_{22}V(n) + a_{23}P(n) + G^*(U(n), V(n), P(n)), \\ P(n+1) = a_{31}U(n) + a_{32}V(n) + a_{33}P(n), \end{cases} \tag{9}$$

where

$$\begin{aligned} &F^*(U(n), V(n), P(n)) \\ &= a_{14}U^2(n) + a_{15}U(n)V(n) + a_{16}U(n)P(n) + a_{17}V(n)P(n) \\ &\quad + a_{18}V^2(n) + a_{19}P^2(n) + b_{11}U^3(n) + b_{12}U^2(n)V(n) + b_{13}U^2(n)P(n) \\ &\quad + b_{14}U(n)V^2(n) + b_{15}U(n)P^2(n) + c_{11}V^2(n)P(n) + c_{12}V(n)P^2(n) \\ &\quad + c_{13}U(n)V(n)P(n) + c_{14}V^3(n) + c_{15}P^3(n) \\ &\quad + o((|U(n)| + |V(n)| + |P(n)|)^3), \end{aligned} \tag{10}$$

$$\begin{aligned} &G^*(U(n), V(n), P(n)) \\ &= a_{24}U^2(n) + a_{25}U(n)V(n) + a_{26}U(n)P(n) + a_{27}V(n)P(n) \\ &\quad + a_{28}V^2(n) + a_{29}P^2(n) + b_{21}U^3(n) + b_{22}U^2(n)V(n) + b_{23}U^2(n)P(n) \\ &\quad + b_{24}U(n)V^2(n) + b_{25}U(n)P^2(n) + c_{21}V^2(n)P(n) + c_{22}V(n)P^2(n) \\ &\quad + c_{23}U(n)V(n)P(n) + c_{24}V^3(n) + c_{25}P^3(n) \\ &\quad + o((|U(n)| + |V(n)| + |P(n)|)^3), \end{aligned} \tag{11}$$

and

$$\begin{aligned} a_{11} &= 1 - h^*(d_1 + a_1), & a_{12} &= -h^* a_2, \\ a_{13} &= h^* \sigma + ha_3, & a_{14} &= h^* \lambda \frac{I^*(I^* + R^*)}{N^{*3}}, \\ a_{15} &= -h^* \lambda \frac{N^*(2I^* + R^*) - 2I^*(I^* + R^*)}{N^{*3}}, & a_{16} &= -h^* \lambda \frac{I^*(S^* - I^* - R^*)}{N^{*3}}, \\ a_{17} &= -h^* \lambda \frac{S^*(I^* - S^* - R^*)}{N^{*3}}, & a_{18} &= h^* \lambda \frac{S^*(S^* + R^*)}{N^{*3}}, \\ a_{19} &= -h^* \lambda \frac{S^* I^*}{N^{*3}}, & b_{11} &= -h^* \lambda \frac{I^*(I^* + R^*)}{N^{*4}}, \\ b_{12} &= h^* \lambda \frac{N^*(2I^* + R^*) - 3I^*(I^* + R^*)}{N^{*4}}, & b_{13} &= h^* \lambda \frac{I^* N^* - 3I^*(I^* + R^*)}{N^{*4}}, \\ b_{14} &= h^* \lambda \frac{N^*(2S^* + R^*) - 3S^*(S^* + R^*)}{N^{*4}}, & b_{15} &= -h^* \lambda \frac{I^* N^* - 3S^* I^*}{N^{*4}}, \\ c_{11} &= h^* \lambda \frac{S^* N^* - 3S^*(S^* + R^*)}{N^{*4}}, & c_{12} &= -h^* \lambda \frac{S^* N^* - 3S^* I^*}{N^{*4}}, \\ c_{13} &= -h^* \lambda \frac{N^*(R^* + N^*) - 3(S^* R^* + I^* R^* + R^{*2} + 2S^* I^*)}{N^{*4}}, \end{aligned}$$

$$\begin{aligned}
 c_{14} &= -h^* \lambda \frac{S^*(S^* + R^*)}{N^{*4}}, & c_{15} &= h^* \lambda \frac{S^* I^*}{N^{*4}}, \\
 a_{21} &= h^* a_1, & a_{22} &= 1 - h^*(d_2 + \gamma) + h^* a_2, \\
 a_{23} &= -h_0 a_3, & a_{2i} &= -a_{1i}, \\
 b_{2j} &= -b_{1j}, & c_{2j} &= -c_{1j} \quad (i = 4, \dots, 9, j = 1, \dots, 5), \\
 a_{31} &= 0, & a_{32} &= h^* \gamma, & a_{33} &= 1 - h^*(d_3 + \sigma).
 \end{aligned}$$

Let

$$T = \begin{pmatrix} t_{11} & t_{12} & t_{13} \\ 1 & 0 & 1 \\ t_{31} & t_{32} & t_{33} \end{pmatrix},$$

where

$$\begin{aligned}
 t_{11} &= A_1 C_1 - B_1 D_1, & t_{12} &= A_1 D_1 + B_1 C_1, \\
 A_1 &= a_{12} + \frac{a_{13} a_{32} (\alpha - a_{33})}{\beta^2 + (\alpha^2 - a_{33})^2}, & B_1 &= \frac{a_{13} a_{32} \beta}{\beta^2 + (\alpha^2 - a_{33})^2}, \\
 C_1 &= \frac{\alpha - a_{11}}{\beta^2 + (\alpha^2 - a_{11})^2}, & D_1 &= \frac{\beta}{\beta^2 + (\alpha^2 - a_{11})^2}, \\
 t_{13} &= \frac{a_{13} a_{32} - a_{12} (b_3 + a_{33})}{(b_3 + a_{11})(b_3 + a_{33})}, & t_{31} &= \frac{a_{32} (\alpha - a_{33})}{\beta^2 + (\alpha^2 - a_{33})^2}, \\
 t_{32} &= \frac{a_{32} \beta}{\beta^2 + (\alpha^2 - a_{33})^2}, & t_{33} &= -\frac{a_{32}}{b_3 + a_{33}}.
 \end{aligned}$$

It is obvious that  $T$  is invertible and

$$\det T = t_{12} t_{31} + t_{13} t_{32} - t_{11} t_{32} - t_{12} t_{33}.$$

Using a translation,

$$\begin{pmatrix} U(n) \\ V(n) \\ P(n) \end{pmatrix} = T \begin{pmatrix} X_n \\ Y_n \\ Z_n \end{pmatrix},$$

then model (9) becomes

$$\begin{cases} X_{n+1} = \alpha X_n - \beta Y_n + F(X_n, Y_n, Z_n), \\ Y_{n+1} = \beta X_n + \alpha Y_n + G(X_n, Y_n, Z_n), \\ Z_{n+1} = -b_3 Z_n + H(X_n, Y_n, Z_n), \end{cases} \tag{12}$$

where

$$\begin{aligned}
 F(X_n, Y_n, Z_n) &= [-t_{32} F^*(U(n), V(n), P(n)) \\
 &\quad + (t_{13} t_{32} - t_{12} t_{33}) G^*(U(n), V(n), P(n))] (\det T)^{-1},
 \end{aligned}$$

$$\begin{aligned}
 G(X_n, Y_n, Z_n) &= [(t_{31} - t_{33})F^*(U(n), V(n), P(n)) \\
 &\quad + (t_{11}t_{33} - t_{13}t_{31})G^*(U(n), V(n), P(n))](\det T)^{-1}, \\
 H(X_n, Y_n, Z_n) &= [t_{32}F^*(U(n), V(n), P(n)) \\
 &\quad + (t_{12}t_{31} - t_{11}t_{32})G^*(U(n), V(n), P(n))](\det T)^{-1},
 \end{aligned}$$

and  $F^*(U(n), V(n), P(n))$ ,  $G^*(U(n), V(n), P(n))$  are given in (10) and (11).

From the above translation we further obtain

$$\begin{aligned}
 F_{X_n X_n} &= F_{X_n X_n}(0, 0, 0) \\
 &= [-(t_{32} + t_{13}t_{32} - t_{12}t_{33})(a_{14}t_{11}^2 + a_{15}t_{11} \\
 &\quad + a_{16}t_{11}t_{31} + a_{17}t_{31} + a_{18} + a_{19}t_{31}^2)](\det T)^{-1}, \\
 F_{Y_n Y_n} &= F_{Y_n Y_n}(0, 0, 0) \\
 &= [-(t_{32} + t_{13}t_{32} - t_{12}t_{33})(a_{14}t_{12}^2 + a_{16}t_{12}t_{32} + a_{19}t_{32}^2)](\det T)^{-1}, \\
 G_{X_n X_n} &= G_{X_n X_n}(0, 0, 0) \\
 &= [(t_{31} + t_{13}t_{31} - t_{33} - t_{11}t_{33})(a_{14}t_{11}^2 + a_{15}t_{11} \\
 &\quad + a_{16}t_{11}t_{31} + a_{17}t_{31} + a_{18} + a_{19}t_{31}^2)](\det T)^{-1}, \\
 G_{Y_n Y_n} &= G_{Y_n Y_n}(0, 0, 0) \\
 &= [(t_{31} + t_{13}t_{31} - t_{33} - t_{11}t_{33})(a_{14}t_{12}^2 + a_{16}t_{12}t_{32} + a_{19}t_{32}^2)](\det T)^{-1}, \\
 H_{X_n X_n} &= H_{X_n X_n}(0, 0, 0) \\
 &= [(t_{32} + t_{11}t_{32} - t_{12}t_{31})(a_{14}t_{11}^2 + a_{15}t_{11} \\
 &\quad + a_{16}t_{11}t_{31} + a_{17}t_{31} + a_{18} + a_{19}t_{31}^2)](\det T)^{-1}, \\
 H_{Y_n Y_n} &= H_{Y_n Y_n}(0, 0, 0) \\
 &= [(t_{32} + t_{11}t_{32} - t_{12}t_{31})(a_{14}t_{12}^2 + a_{16}t_{12}t_{32} + a_{19}t_{32}^2)](\det T)^{-1}, \\
 F_{X_n Y_n} &= F_{X_n Y_n}(0, 0, 0) \\
 &= [-(t_{32} + t_{13}t_{32} - t_{12}t_{33})(2a_{14}t_{11}t_{12} + a_{15}t_{12} \\
 &\quad + a_{16}(t_{11}t_{32} + t_{12}t_{31}) + a_{17}t_{32} + 2a_{19}t_{31}t_{32})](\det T)^{-1}, \\
 G_{X_n Y_n} &= G_{X_n Y_n}(0, 0, 0) \\
 &= [(t_{31} + t_{13}t_{31} - t_{33} - t_{11}t_{33})(2a_{14}t_{11}t_{12} + a_{15}t_{12}, \\
 &\quad + a_{16}(t_{11}t_{32} + t_{12}t_{31}) + a_{17}t_{32} + 2a_{19}t_{31}t_{32})](\det T)^{-1}, \\
 H_{X_n Y_n} &= H_{X_n Y_n}(0, 0, 0) \\
 &= [(t_{32} + t_{11}t_{32} - t_{12}t_{31})(2a_{14}t_{11}t_{12} + a_{15}t_{12} \\
 &\quad + a_{16}(t_{11}t_{32} + t_{12}t_{31}) + a_{17}t_{32} + 2a_{19}t_{31}t_{32})](\det T)^{-1}, \\
 F_{X_n Z_n} &= F_{X_n Z_n}(0, 0, 0) \\
 &= [-(t_{32} + t_{13}t_{32} - t_{12}t_{33})(2a_{14}t_{11}t_{13} + a_{15}(t_{11} + t_{13}))
 \end{aligned}$$



$$\begin{aligned}
 & + a_{16}(t_{11}t_{33} + t_{13}t_{31}) + a_{17}(t_{31} + t_{33}) + 2a_{18} + 2a_{19}t_{31}t_{33} \Big] (\det T)^{-1}, \\
 G_{X_n Z_n} &= G_{X_n Z_n}(0, 0, 0) \\
 &= \Big[ (t_{31} + t_{13}t_{31} - t_{33} - t_{11}t_{33})(2a_{14}t_{11}t_{13} + a_{15}(t_{11} + t_{13}) \\
 & \quad + a_{16}(t_{11}t_{33} + t_{13}t_{31}) + a_{17}(t_{31} + t_{33}) + 2a_{18} + 2a_{19}t_{31}t_{33}) \Big] (\det T)^{-1}, \\
 F_{Y_n Z_n} &= F_{Y_n Z_n}(0, 0, 0) \\
 &= \Big[ -(t_{32} + t_{13}t_{32} - t_{12}t_{33})(2a_{14}t_{12}t_{13} + a_{15}t_{12} \\
 & \quad + a_{16}(t_{12}t_{33} + t_{13}t_{32}) + a_{17}t_{32} + 2a_{19}t_{32}t_{33}) \Big] (\det T)^{-1}, \\
 G_{Y_n Z_n} &= G_{Y_n Z_n}(0, 0, 0) \\
 &= \Big[ (t_{31} + t_{13}t_{31} - t_{33} - t_{11}t_{33})(2a_{14}t_{12}t_{13} + a_{15}t_{12} \\
 & \quad + a_{16}(t_{12}t_{33} + t_{13}t_{32}) + a_{17}t_{32} + 2a_{19}t_{32}t_{33}) \Big] (\det T)^{-1}, \\
 F_{X_n X_n X_n} &= F_{X_n X_n X_n}(0, 0, 0) \\
 &= \Big[ -(t_{32} + t_{13}t_{32} - t_{12}t_{33})(b_{11}t_{11}^3 + b_{12}t_{11}^2 + b_{13}t_{11}^2 t_{31} + b_{14}t_{11} \\
 & \quad + b_{15}t_{11}t_{31}^2 + c_{11}t_{31} + c_{12}t_{31}^2 + c_{13}t_{11}t_{13} + c_{14} + c_{15}t_{31}^3) \Big] (\det T)^{-1}, \\
 G_{X_n X_n X_n} &= G_{X_n X_n X_n}(0, 0, 0) \\
 &= \Big[ (t_{31} + t_{13}t_{31} - t_{33} - t_{11}t_{33})(b_{11}t_{11}^3 + b_{12}t_{11}^2 + b_{13}t_{11}^2 t_{31} + b_{14}t_{11} \\
 & \quad + b_{15}t_{11}t_{31}^2 + c_{11}t_{31} + c_{12}t_{31}^2 + c_{13}t_{11}t_{13} + c_{14} + c_{15}t_{31}^3) \Big] (\det T)^{-1}, \\
 F_{Y_n Y_n Y_n} &= F_{Y_n Y_n Y_n}(0, 0, 0) \\
 &= \Big[ -(t_{32} + t_{13}t_{32} - t_{12}t_{33})(b_{11}t_{12}^3 + b_{13}t_{12}^2 t_{32} \\
 & \quad + b_{15}t_{12}t_{32}^2 + c_{15}t_{32}^3) \Big] (\det T)^{-1}, \\
 G_{Y_n Y_n Y_n} &= G_{Y_n Y_n Y_n}(0, 0, 0) \\
 &= \Big[ (t_{31} + t_{13}t_{31} - t_{33} - t_{11}t_{33})(b_{11}t_{12}^3 \\
 & \quad + b_{13}t_{12}^2 t_{32} + b_{15}t_{12}t_{32}^2 + c_{15}t_{32}^3) \Big] (\det T)^{-1}, \\
 F_{X_n X_n Y_n} &= F_{X_n X_n Y_n}(0, 0, 0) \\
 &= \Big\{ -(t_{32} + t_{13}t_{32} - t_{12}t_{33}) \Big[ 3b_{11}t_{11}^2 t_{12} + 2b_{12}t_{11}t_{12} \\
 & \quad + b_{13}(t_{11}^2 t_{32} + 2t_{11}t_{13}t_{31}) + b_{14}t_{12} + b_{15}(t_{12}t_{31}^2 + 2t_{11}t_{31}t_{32}) \\
 & \quad + c_{11}t_{32}^2 + 2c_{12}t_{31}t_{32} + c_{13}(t_{11}t_{32} + t_{12}t_{31}) + 3c_{15}t_{31}^2 t_{32} \Big] \Big\} (\det T)^{-1}, \\
 G_{X_n X_n Y_n} &= G_{X_n X_n Y_n}(0, 0, 0) \\
 &= \Big\{ (t_{31} + t_{13}t_{31} - t_{33} - t_{11}t_{33}) \Big[ 3b_{11}t_{11}^2 t_{12} + 2b_{12}t_{11}t_{12} \\
 & \quad + b_{13}(t_{11}^2 t_{32} + 2t_{11}t_{13}t_{31}) + b_{14}t_{12} + b_{15}(t_{12}t_{31}^2 + 2t_{11}t_{31}t_{32}) \\
 & \quad + c_{11}t_{32}^2 + 2c_{12}t_{31}t_{32} + c_{13}(t_{11}t_{32} + t_{12}t_{31}) + 3c_{15}t_{31}^2 t_{32} \Big] \Big\} (\det T)^{-1}, \\
 F_{X_n Y_n Y_n} &= F_{X_n Y_n Y_n}(0, 0, 0) \\
 &= \Big\{ -(t_{32} + t_{13}t_{32} - t_{12}t_{33}) \Big[ 3b_{11}t_{11}t_{12}^2 + b_{12}t_{12}^2 \\
 & \quad + b_{13}(t_{12}^2 t_{31} + 2t_{11}t_{12}t_{32}) + b_{15}(t_{11}t_{32}^2 + 2t_{12}t_{31}t_{32}) \Big] \Big\}
 \end{aligned}$$

$$\begin{aligned}
 &+ c_{12}t_{32}^2 + c_{13}t_{12}t_{32} + 3c_{15}t_{31}t_{32}^2 \} (\det T)^{-1}, \\
 G_{X_n Y_n Y_n} &= G_{X_n Y_n Y_n}(0, 0, 0) \\
 &= \{ (t_{31} + t_{13}t_{31} - t_{33} - t_{11}t_{33}) [3b_{11}t_{11}t_{12}^2 + b_{12}t_{12}^2 \\
 &\quad + b_{13}(t_{12}^2 t_{31} + 2t_{11}t_{12}t_{32}) + b_{15}(t_{11}t_{32}^2 + 2t_{12}t_{31}t_{32}) \\
 &\quad + c_{12}t_{32}^2 + c_{13}t_{12}t_{32} + 3c_{15}t_{31}t_{32}^2] \} (\det T)^{-1}.
 \end{aligned}$$

In order for the system to undergo the Hopf bifurcation of model (12), we let

$$\begin{aligned}
 g_{11} &= \frac{1}{4} [F_{X_n X_n} + F_{Y_n Y_n} + i(G_{X_n X_n} + G_{Y_n Y_n})], \\
 g_{02} &= \frac{1}{4} [F_{X_n X_n} - F_{Y_n Y_n} - 2G_{X_n Y_n} + i(G_{X_n X_n} - G_{Y_n Y_n} + 2F_{X_n Y_n})], \\
 g_{20} &= \frac{1}{4} [F_{X_n X_n} - F_{Y_n Y_n} + 2G_{X_n Y_n} + i(G_{X_n X_n} - G_{Y_n Y_n} - 2F_{X_n Y_n})], \\
 G_{21} &= \frac{1}{8} [F_{X_n X_n X_n} + F_{X_n Y_n Y_n} + G_{X_n X_n Y_n} + G_{Y_n Y_n Y_n} \\
 &\quad + i(G_{X_n X_n X_n} + G_{X_n Y_n Y_n} - F_{X_n X_n Y_n} - F_{Y_n Y_n Y_n})], \\
 h_{11} &= \frac{1}{4} (H_{X_n X_n} + H_{Y_n Y_n}), \\
 h_{20} &= \frac{1}{4} (H_{X_n X_n} - H_{Y_n Y_n} - 2iH_{X_n Y_n}), \\
 G_{110} &= \frac{1}{2} [F_{X_n Z_n} + G_{Y_n Z_n} + i(G_{X_n Z_n} - F_{Y_n Z_n})], \\
 G_{101} &= \frac{1}{2} [F_{X_n Z_n} - G_{Y_n Z_n} + i(F_{Y_n Z_n} + G_{X_n Z_n})], \\
 w_{11} &= \frac{h_{11}}{b_3}, \quad w_{20} = \frac{h_{20}}{b_3 + 2i\beta}, \\
 g_{21} &= G_{21} + (2w_{11}G_{110} + w_{20}G_{101}).
 \end{aligned}$$

Further, we let

$$c_1(0) = \frac{i}{2\beta} \left( g_{20}g_{11} - 2|g_{11}|^2 - \frac{1}{3}|g_{02}|^2 \right) + \frac{1}{2}g_{21}$$

and

$$\mu_2 = -\frac{\operatorname{Re}(c_1(0))}{\operatorname{Re}(w_{n^*})}, \quad \beta_2 = 2 \operatorname{Re}(c_1(0)).$$

Now by the Hopf theorem of [36] we can obtain the main result of this section.

**Theorem 2** *If conditions (7), (8) hold and  $\mu_2 \neq 0$ , then model (4) undergoes a Hopf bifurcation at equilibrium  $E^*(S^*, I^*, R^*)$  when the parameter  $h^{**}$  changes in a small neighborhood of the origin. The direction of the Hopf bifurcation of model (4) is determined by the sign of  $\mu_2$ : if  $\mu_2 > 0$  ( $\mu_2 < 0$ ), then the Hopf bifurcation is supercritical (subcritical) and the*

*bifurcating periodic solutions exist for  $h > h^*$  ( $h < h^*$ ).  $\beta_2$  determines the stability of the bifurcating periodic solutions: the bifurcating periodic solutions are stable (unstable) if  $\beta_2 < 0$  ( $\beta_2 > 0$ ).*

**Remark 1** In [14], the authors carried out numerical simulations to obtain a Hopf bifurcation. On the contrary, in this paper, we use the bifurcation theorem to prove the existence, stability, and direction of the Hopf bifurcation of a three-dimensional discrete-time *SIRS* epidemic model. The main results in this paper also solve the open problem in [37].

**Remark 2** In [15–17, 23–26], the authors only considered a two-dimensional discrete-time epidemic model. As is well known, the diseases are spreading in different populations, such as susceptible individuals *S*, infective individuals *I*, and recovered individuals *R*. For better understanding the pathogenesis and the spread of the disease process, a higher-dimensional epidemic model should be studied. Therefore, in this paper, we study the Hopf bifurcation and flip bifurcation of a three-dimensional discrete-time *SIRS* epidemic model, which is more realistic for the spread of the disease process.

#### 4 Numerical simulation

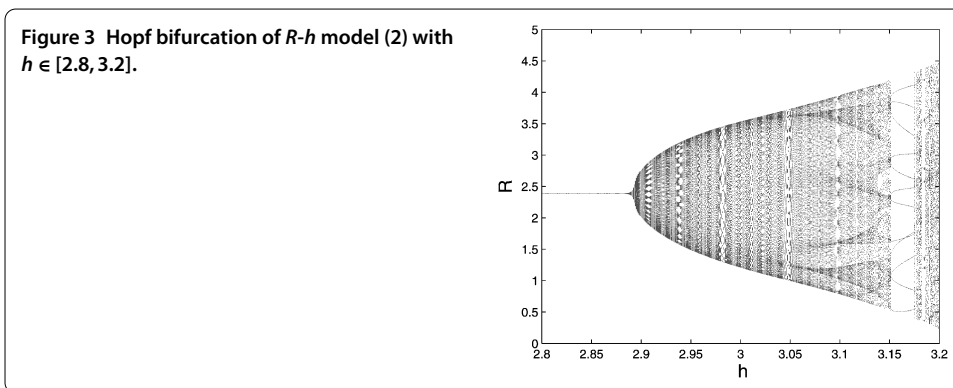
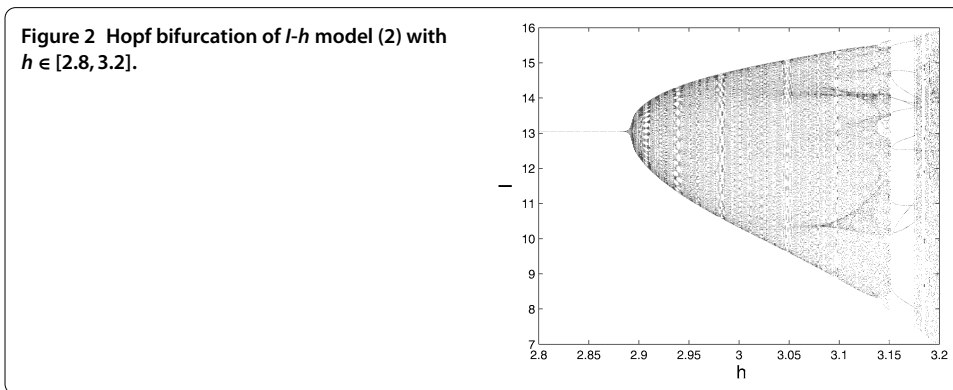
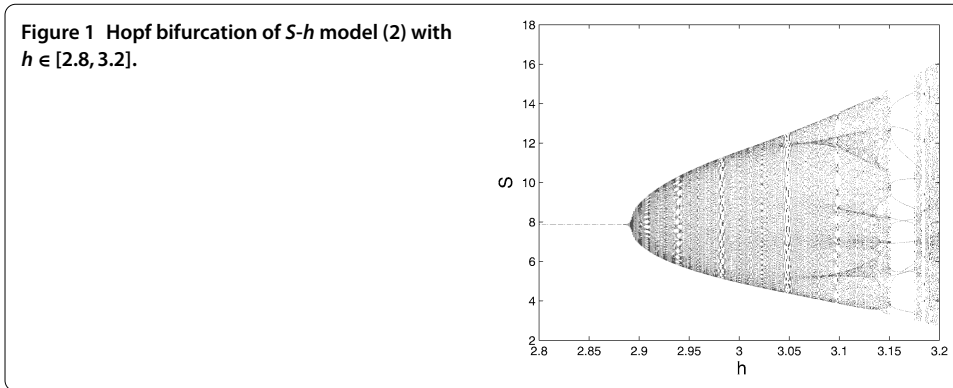
In this section, six examples are provided to illustrate our theoretical results in Theorem 2. In Examples 1 and 2, the time step size *h* is selected as the bifurcation parameter. The first one shows the Hopf bifurcation diagrams and the corresponding phase portraits of model (2) to confirm the above theoretical analysis, and it indicates new interesting complex dynamical behaviors. In the third section we have not proven the existence of the flip bifurcation of model (2). Therefore, the second example is about the flip bifurcation of model (2), which is only obtained by using numerical simulations. The adequate contact rate  $\lambda$  and the death rate  $d_2$  have a significant role to play in the disease spreading in model (2). Hence,  $\lambda$  and  $d_2$  also are chosen as the bifurcation parameter in Examples 3-6 to detect the bifurcation and chaos behaviors.

**Example 1** We choose  $A = 2.4$ ,  $d_1 = 0.1$ ,  $d_2 = 0.12$ ,  $d_3 = 0.02$ ,  $\lambda = 0.8$ ,  $\gamma = 0.15$ ,  $\sigma = 0.8$ ,  $h \in [2.6, 3.2]$ , and the initial values  $(S_0, I_0, R_0) = (4, 3.2, 0.5)$ . By computing we obtain the basic reproductive rate  $\mathfrak{R}_0 = \frac{80}{27} > 1$ ,  $E^*(S^*, I^*, R^*) = (7.8637, 13.0491, 2.370)$ . When  $h^* = 2.8903$ , we obtain  $\Delta = 22.4462 > 0$ , which implies that the Jacobian matrix  $J(E^*)$  has three eigenvalues,  $w_1 = 0.6923$ ,  $w_{2,3} = \alpha \pm \beta i = -0.8388 \pm 0.5444i$  with  $|w_{2,3}| = 1$ . Further, by simple computing, we obtain  $k = 0.5289$  and

$$\alpha = -0.8388 \neq -\frac{1}{2}, \quad \beta = 0.5444 \neq \pm \frac{\sqrt{3}}{2}, \quad (\alpha^2 - \beta^2)^2 - 2\alpha\beta = 1.0791 \neq 1.$$

Then conditions (6), (7) hold and  $\mu_2 = 9.2025 \times 10^{-4} \neq 0$ , which indicates that there exists a Hopf bifurcation of model (2). Since  $\beta_2 = -0.002$  and  $\mu_2 = 9.2025 \times 10^{-4}$ , the Hopf bifurcation is stable and supercritical (see Figures 1-3).

Figures 1-3 show that the endemic equilibrium  $E^*(7.8637, 13.0491, 2.370)$  of model (2) is stable for  $h < 2.8903$ , and it loses its stability when  $h = 2.8903$ ; moreover, when  $h > 2.8903$  there appear complex dynamical behaviors. For example, when the time step size *h* changes from 3.155 to 3.179 there appear period-12 orbits, and when the step size *h* increases continuously there appear chaos and period-7 orbits, which can be found in the phase portraits.



The phase portraits (Figures 4-11) of the bifurcation diagrams (Figures 1-3) provide detailed information about the dynamical behaviors changing from a stable equilibrium to Hopf bifurcation, chaos, and then more complex dynamical behaviors. Figure 4 shows when  $h = 2.86 < 2.8903$ , then the endemic equilibrium  $E^*(7.8637, 13.0491, 2.370)$  has local stability. Following the increase of  $h$  there exists a stable periodical solution, that is, the Hopf bifurcation which can be seen in Figure 5. When  $h$  continues becoming bigger the stable invariant circle is broken slowly and there appear more than one periodical attractors from Figures 6-11. The period-12 orbits and period-7 orbits can be found in Figures 8 and 10, respectively. Furthermore, there exist more complex dynamical behaviors when  $h$  is much bigger as in Figure 11.

**Figure 4**  $h = 2.86$ .

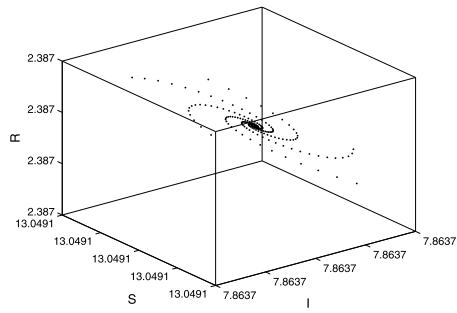


**Figure 5**  $h = 2.9$ .

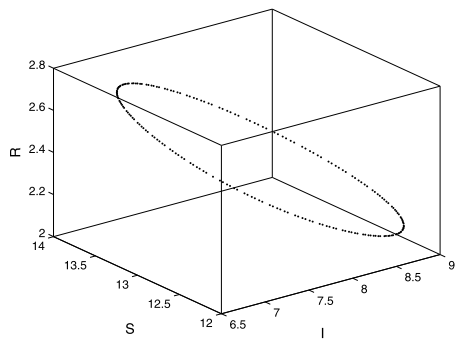


**Figure 6**  $h = 3.138$ .

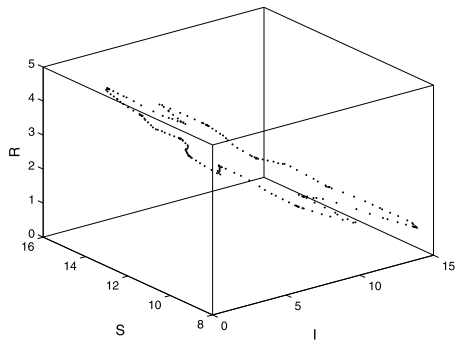


**Figure 7**  $h = 3.15$ .

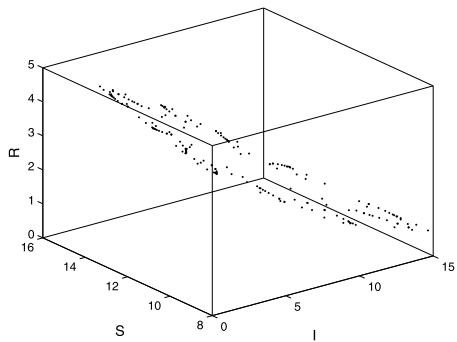


**Figure 8**  $h = 3.155$ .

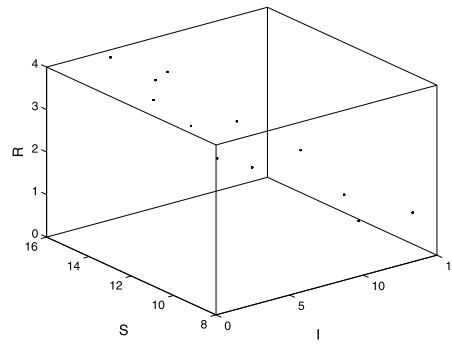


**Figure 9**  $h = 3.179$ .

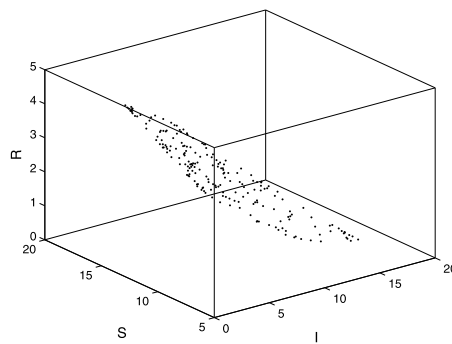


**Figure 10**  $h = 3.183$ .

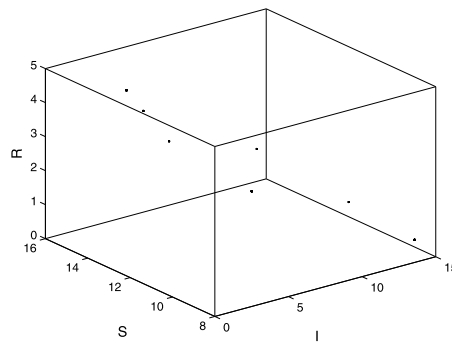
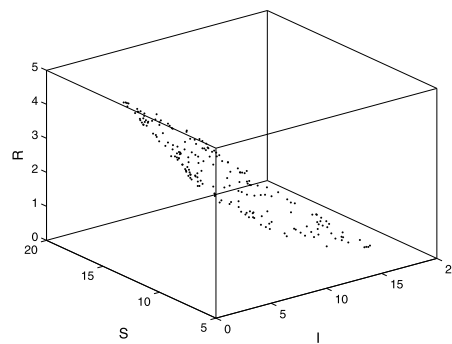


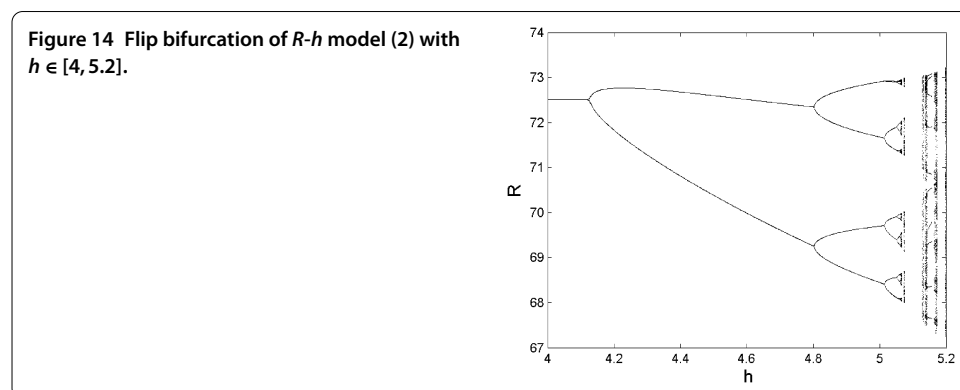
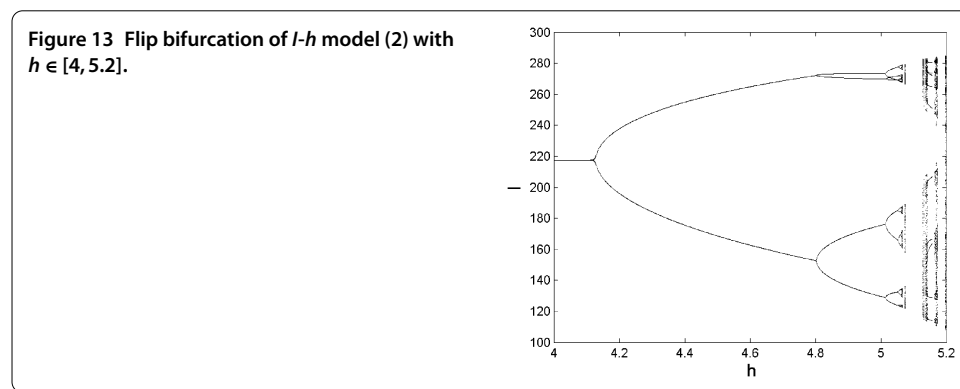
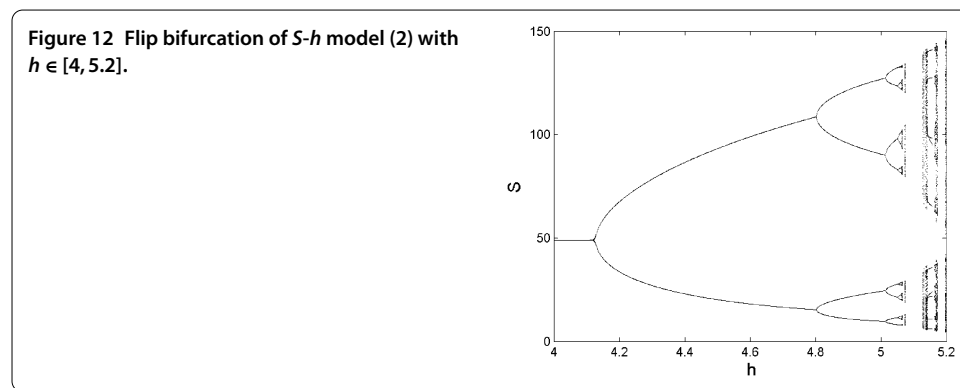
**Figure 11**  $h = 3.2$ .



In the following examples, we only provide the bifurcations diagrams.

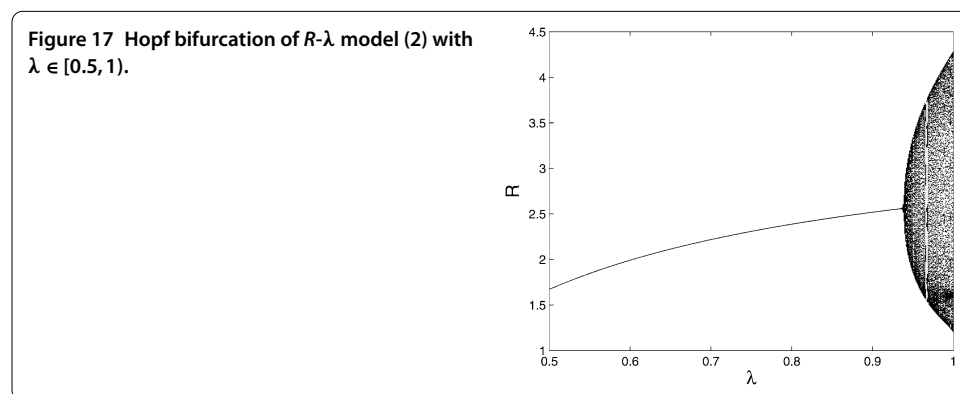
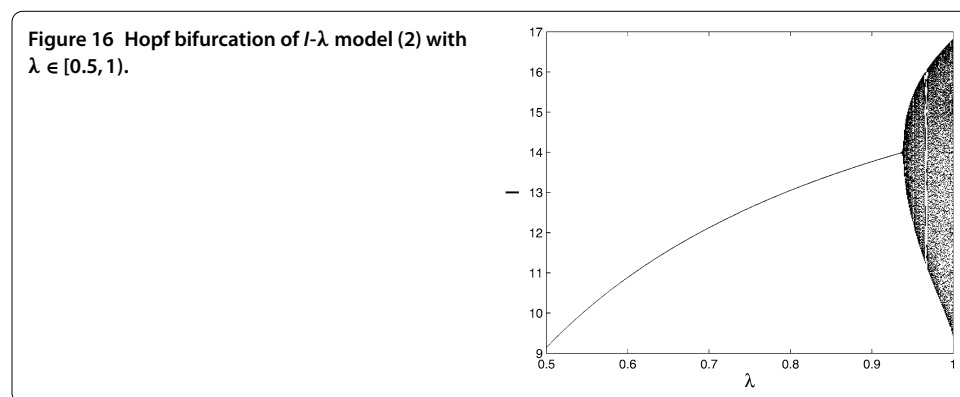
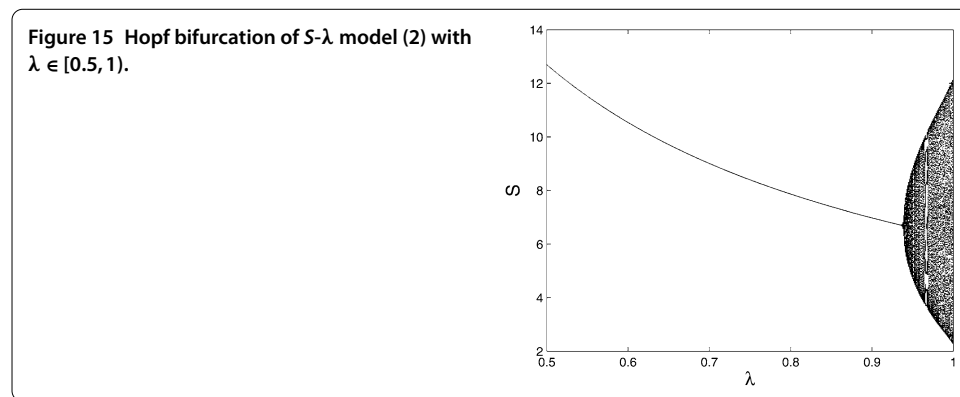
**Example 2** We choose  $A = 30, d_1 = 0.05, d_2 = 0.12, d_3 = 0.02, \lambda = 0.9, \gamma = 0.01, \sigma = 0.01, h \in [4, 5.2]$ , and the initial values  $(S_0, I_0, R_0) = (60, 30, 20)$ . By computing we obtain the basic reproductive rate  $\mathfrak{R}_0 = \frac{90}{13} > 1, E^*(S^*, I^*, R^*) = (48.9642, 217.5141, 72.5047)$ . From the flip bifurcation diagrams (see Figures 12-14), there exists a critical value of  $h$ , and here we denote it by  $h_*$ . When  $h_* = 4.1321$ , we compute that  $\Delta = -4.6930 < 0$  and the three real eigenvalues of the Jacobian matrix  $J(E^*)$  are  $w_1 = -1, w_2 = 0.4062,$  and  $w_3 = 0.8787$ .

Figures 12-14 show that the endemic equilibrium  $E^*(48.9642, 217.5141, 72.5047)$  of model (2) is stable for  $h < h_* = 4.1321$  and loses its stability when  $h = h_* = 4.1321$ . The flip bifurcation and chaotic behaviors appear when  $h > h_*$ . In detail, the period-2 orbits ap-



pear when  $h$  is approximatively changing in  $(4.1321, 4.8]$ ; the period-4 orbits appear when  $h$  goes from 4.8 to 5.01, and following the increase of  $h$ , model (2) undergoes period-8, -16, and quasi-periodic orbits, and chaos sets in ultimately.

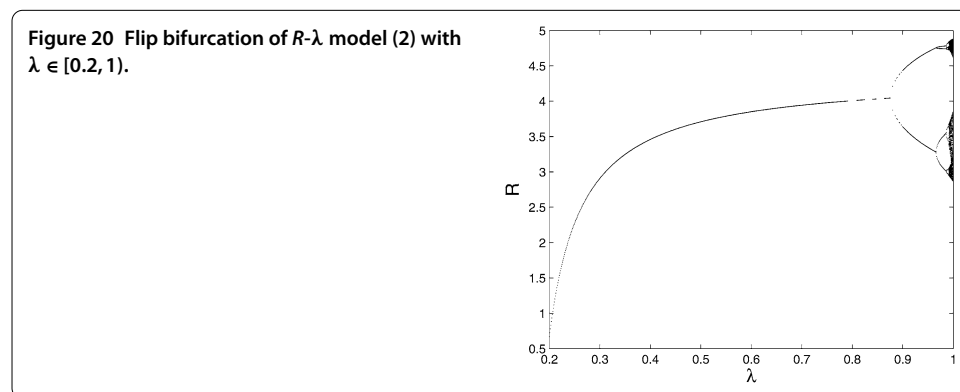
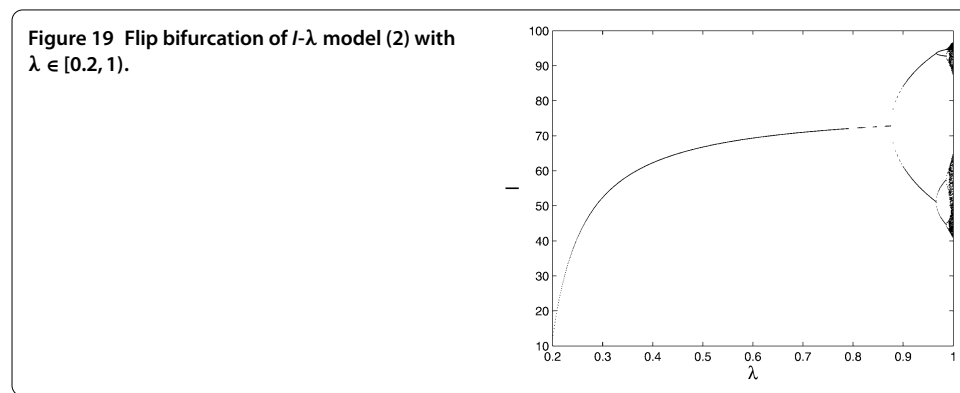
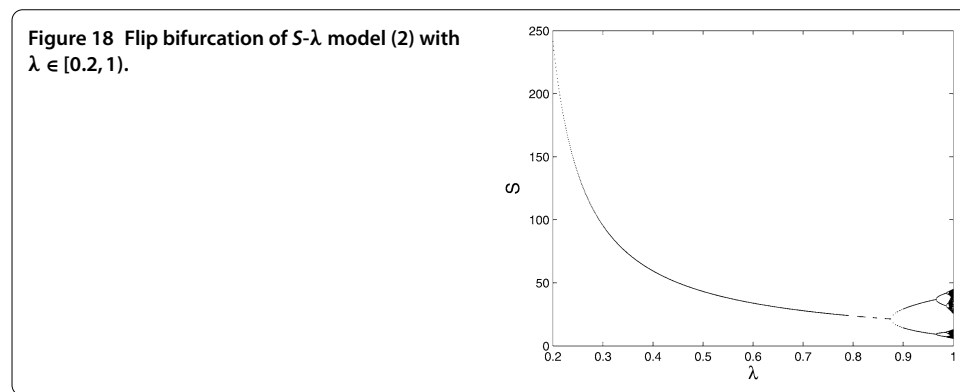
**Example 3** We choose  $h = 2.5$ ,  $A = 2.4$ ,  $d_1 = 0.1$ ,  $d_2 = 0.12$ ,  $d_3 = 0.02$ ,  $\gamma = 0.15$ ,  $\sigma = 0.8$ ,  $\lambda \in [0.5, 1)$ , and the initial values  $(S_0, I_0, R_0) = (4, 3.2, 0.5)$ . By computing we obtain the basic reproductive rate  $\mathfrak{R}_0 = \frac{100\lambda}{27}$ . From  $\lambda \in [0.5, 1)$ , then we have  $\mathfrak{R}_0 = \frac{100\lambda}{27} > 1$ . Therefore, there exists an endemic equilibrium  $E^*(S^*, I^*, R^*)$ , which is a function of  $\lambda$ . Figure 15 illustrates that when the disease contact rate  $\lambda$  is smaller than the critical value  $\lambda^* \approx 0.945$  the equilibrium values of  $S$  are locally stable. It is increasing for  $I_n$  and  $R_n$  when  $\lambda \in [0.5, \lambda^*]$



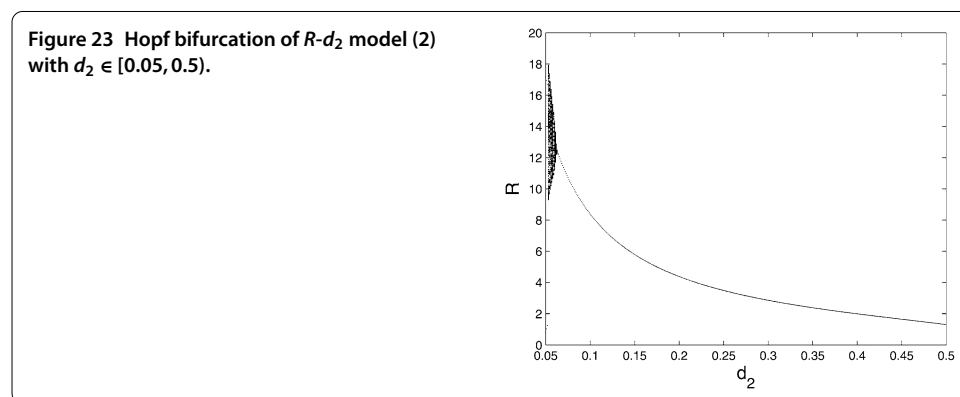
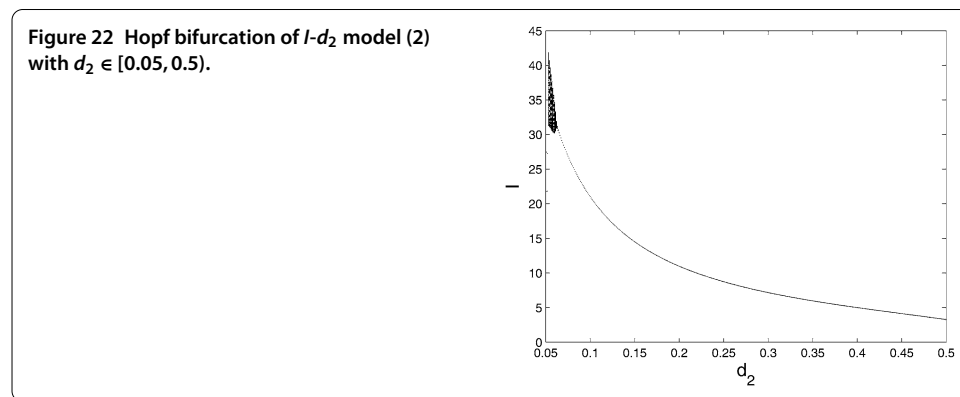
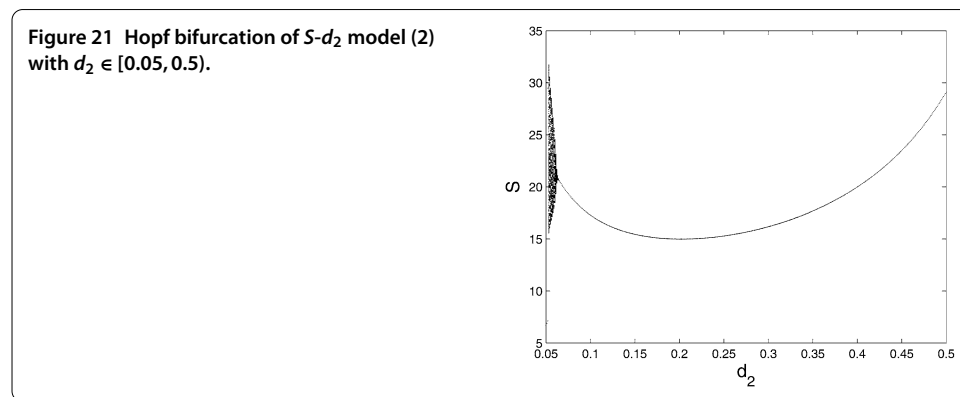


(see Figures 16 and 17). Finally, there appears a Hopf bifurcation for  $S_n, I_n,$  and  $R_n$  when  $\lambda$  is bigger than  $\lambda^*$  (see Figures 15-17).

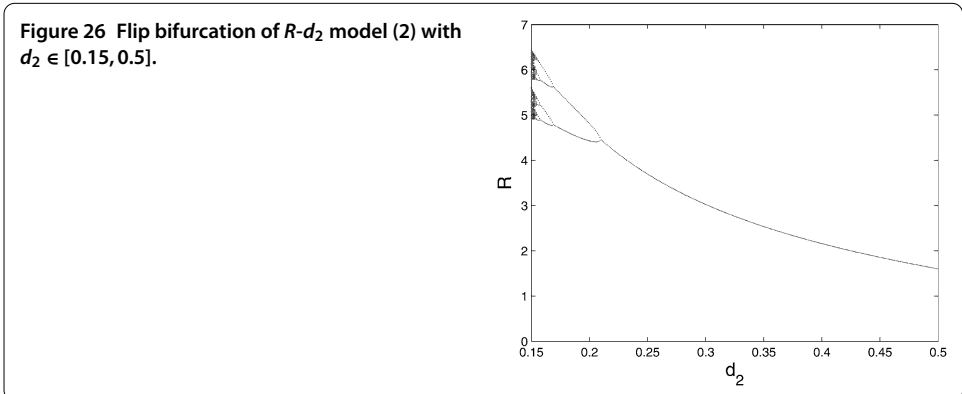
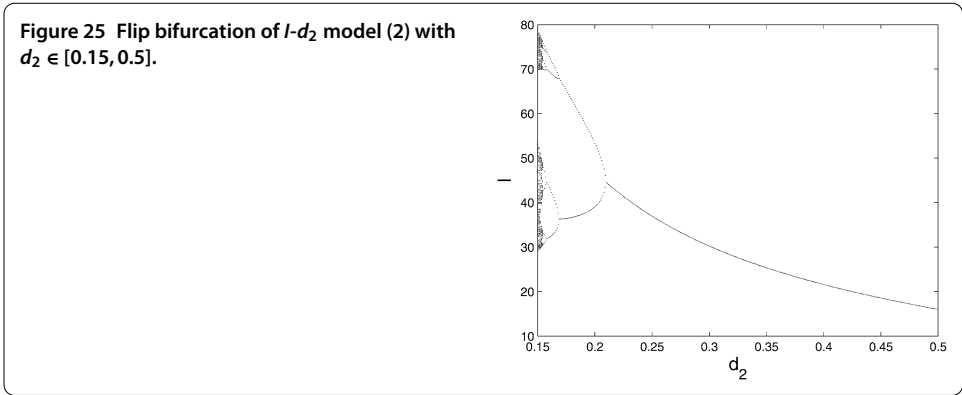
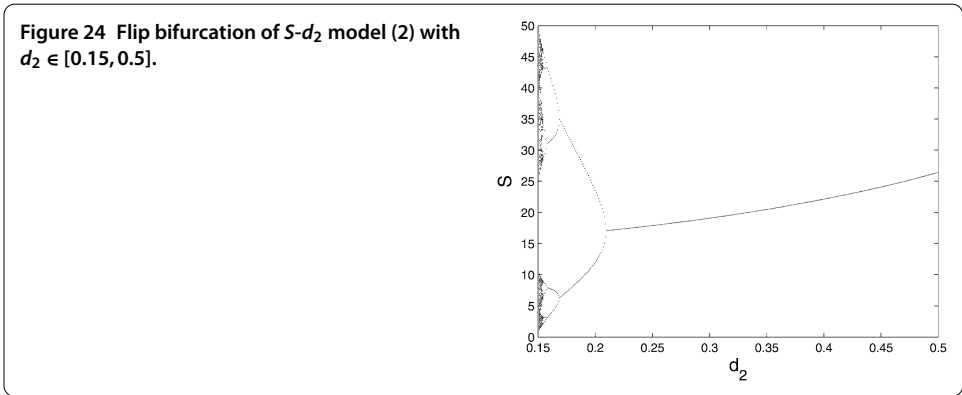
**Example 4** We choose  $h = 4.28, A = 14.25, d_1 = 0.05, d_2 = 0.18, d_3 = 0.02, \gamma = 0.01, \sigma = 0.16, \lambda \in [0.2, 1),$  and the initial values  $(S_0, I_0, R_0) = (60, 30, 20)$ . By computing we obtain the basic reproductive rate  $\mathfrak{R}_0 = \frac{100\lambda}{19}$ . Since  $\lambda \in [0.2, 1)$ , then we have  $\mathfrak{R}_0 = \frac{100\lambda}{19} > 1$ . As in Example 3, the endemic equilibrium  $E^*(S^*, I^*, R^*)$  exists and is a function of  $\lambda$ . From Figures 18-20, we see that the equilibrium values of  $S, I,$  and  $R,$  which are locally stable when  $\lambda$  is smaller than the critical value  $\lambda^* \approx 0.875$  (see Figures 18-20). When  $\lambda$  is bigger than  $\lambda^* \approx 0.875$  there appears a flip bifurcation, and model (2) undergoes chaotic behaviors with the continuous increasing of  $\lambda$ .



**Example 5** We choose  $h = 3.2$ ,  $A = 2.8$ ,  $d_1 = 0.04$ ,  $d_3 = 0.001$ ,  $\lambda = 0.81$ ,  $\gamma = 0.2$ ,  $\sigma = 0.5$ ,  $d_2 \in [0.05, 0.5]$ , and the initial values  $(S_0, I_0, R_0) = (4, 3.2, 0.85)$ . By computing we obtain the basic reproductive rate  $\mathfrak{R}_0 = \frac{81}{100d_2+20}$ . From  $d_2 \in [0.05, 0.5]$ , we have  $\mathfrak{R}_0 > 1$ . Therefore, there exists an endemic equilibrium  $E^*(S^*, I^*, R^*)$ , which is a function of  $d_2$ . From Figures 21-23, we see that when  $d_2 \approx 0.063$  there appears a Hopf bifurcation for  $S_n$ ,  $I_n$ , and  $R_n$ . When  $d_2$  is bigger than 0.063 the Hopf bifurcation disappears and the endemic equilibrium  $E^*(S^*, I^*, R^*)$  is local stable. But the value change of the three species is different following the changing of  $d_2$ . Particularly, when  $d_2$  is becoming bigger than 0.063 the equilibrium values of  $S$ , which are locally stable (see Figure 21). Since  $d_2$  is the death rate of  $I_n$ , it is certain that  $I_n$  is decreasing following the increasing of  $d_2$  and this results in the decreasing of  $R_n$  (see Figures 22 and 23).



**Example 6** We choose  $h = 4.2, A = 12, d_1 = 0.15, d_3 = 0.02, \lambda = 0.85, \gamma = 0.01, \sigma = 0.08, d_2 \in [0.15, 0.5]$ , and the initial values  $(S_0, I_0, R_0) = (60, 20, 30)$ . By computing we obtain the basic reproductive rate  $\mathfrak{R}_0 = \frac{85}{100d_2+1}$ . One can also obtain  $\mathfrak{R}_0 = \frac{85}{100d_2+1} > 1$  from  $d_2 \in [0.15, 0.5]$ . Therefore, there exists an endemic equilibrium  $E^*(S^*, I^*, R^*)$ , which is a function of  $d_2$ . Figures 24-26 show that model (2) undergoes chaos and flip bifurcation when the death rate  $d_2$  of the infective individuals  $I_n$  varies from 0.15 to 0.5. Particularly, when  $d_2$  varies from 0.15 to the critical value  $d_2^* \approx 0.21$  there appear chaotic behaviors and a flip bifurcation. When  $d_2$  is bigger than  $d_2^*$  the equilibrium values of  $S, I$ , and  $R$ , which are locally stable (see Figures 25 and 26).



**Remark 3** Example 1 shows when the parameters satisfy the conditions in Theorem 2 for model (2) there will appear a Hopf bifurcation from the endemic equilibrium  $E^*(S^*, I^*, R^*)$  (see Figures 1-3). In addition, the flip bifurcation also appears in Example 2 when the step parameter  $h$  is changing at the neighborhood of  $h^*$  (see Figures 12-14). Furthermore, these results indicate that chaos dynamical behaviors of model (2) can be obtained according to the paths of the flip bifurcation and the Hopf bifurcation when the step size  $h$  is changed, and we should control the disease transmitting between the different individuals  $S_n$ ,  $I_n$ , and  $R_n$ .

**Remark 4** The results in Examples 3-6 make it clear that not only the step parameter  $h$  but also the adequate contact rate  $\lambda$  and the death rate  $d_2$  for the individuals  $I_n$  can cause bifurcation behaviors and chaos behaviors for model (2). Controlling the key parameters in the epidemic model has an important role to play in the disease controlling process, such as the adequate contact rate and the death rate. These results are similar to the results in [38].

## 5 Discussion and conclusion

The bifurcation analysis of a three-dimensional discrete *SIRS* epidemic model with standard incidence rate is discussed in this paper. The existence, stability, and bifurcation direction of the Hopf bifurcation are obtained in Theorem 2 by the normal form theorem and bifurcation theory. Further, numerical simulations are used to illustrate our theory results, and some interesting dynamical behaviors (flip bifurcation, Hopf bifurcation, and chaos) of model (2) are also obtained when some key parameters are chosen as the bifurcation parameters (see Figures 1-26).

For analyzing the Hopf bifurcation, we choose the time step parameter  $h$  as the bifurcation parameter, and the existence and direction of the Hopf bifurcation of model (2) are proved by the normal form theorem and bifurcation theory in Theorem 2. Particularly, if the time step parameter  $h$  is sufficient big, then when the basic reproductive rate  $\mathfrak{R}_0 > 1$  and parameters  $(A, d_1, d_2, d_3, h, \lambda, \gamma, \sigma)$  satisfy case (I) in condition (4) of Theorem 3 in [33] model (2) there appears a Hopf bifurcation and chaotic attractors (see Figures 1-3), which implied that the susceptible and infective individuals can coexist in a stable period cycle. Most important is that from the bifurcation figures we can control the parameters  $(A, d_1, d_2, d_3, h, \lambda, \gamma, \sigma)$  to control the disease when the step parameter  $h$  is smaller than the bifurcation values  $h^*$ . In addition, when the step parameter  $h$  changes, flip bifurcation diagrams appear in Example 2 by the numerical simulations (see Figures 12-14). These figures show that there exists a flip bifurcation, which also can result in chaotic behaviors in model (2). This result enriches the dynamical behaviors for model (2).

It is well known that the adequate contact rate  $\lambda$  and the death rate  $d_2$  for the individuals  $I_n$  have a key role to play in the disease transmission. We choose  $\lambda$  as the bifurcation parameters and select some suitable values for the other parameters  $(A, d_1, d_2, d_3, h, \gamma, \sigma)$  and initial values for  $S_0, I_0, R_0$ , then there exist a Hopf bifurcation and a flip bifurcation for model (2), which can be seen from Example 3 and Example 4 (see Figures 15-17 and Figures 18-20). Eventually, there appear chaos dynamical behaviors. And the same results also exist when the death rate  $d_2$  is chosen as the bifurcation parameter in Examples 5 and 6 (see Figures 21-23 and Figures 24-26). These results indicate that the key parameters in the epidemic model will affect the dynamical behaviors significantly, such as the flip bifurcation, the Hopf bifurcation, and chaos, which corresponds with the results in [38].

For comparing with previous work [15–17, 23–26], one only considered the dynamical behaviors for the two-dimensional discrete-time epidemic model. There are few studies of the bifurcation analysis of the three-dimensional discrete-time epidemic model. Since the diseases spread in different populations, such as susceptible individuals  $S$ , infective individuals  $I$ , and recovered individuals  $R$ , the recovered individuals  $R$  can also become susceptible individuals  $S$ , such as in the case of the flue disease. For better understanding the pathogenesis and the spread of the disease process, a higher-dimensional epidemic model should be studied, especially, for the bifurcation and chaos dynamical behaviors studies. Our main results provide important information for the disease control when the disease transmission appears to show complex dynamical behaviors.

However, the disease has a relation with the initial values because Hopf bifurcation and flip bifurcation are local bifurcations. If we obtain the global bifurcation, then the disease has no relation with the initial values. There are still some interesting open problems: whether we can prove the existence of the flip bifurcation, and whether we can find an effective way to prove the global stability of model (2), such as by constructing Lyapunov function. In addition, the Hopf bifurcation is a type codimension-one bifurcation, that is, the bifurcation results by one bifurcation parameter. In [39, 40], the authors discussed the codimension-two bifurcation, which is controlled by two bifurcation parameters. For model (2), one addressed whether there exists a codimension-two bifurcation with the eigenvalues  $w = \pm i, \frac{-1 \pm \sqrt{3}i}{2}$  when two bifurcation parameters are changed. Moreover, other discretization methods (such as the backward Euler method, the nonstandard finite difference scheme) can be used on model (1) to obtain the corresponding discrete model. For the new discrete model, one may ask whether there exist bifurcation and chaos. These issues will be discussed in the future.

Some real data from a known epidemic disease to illustrate the validity of our theoretical results also should be considered in our future work, such as how to predict the occurrence and the controlling of disease, and in which way complex behaviors (including bifurcations, chaos, and strange attractors) have impact on the dynamics of disease.

#### Competing interests

The authors declare that they have no competing interests.

#### Authors' contributions

The authors declare that the study was realized in collaboration with the same responsibility. All authors read and approved the final manuscript.

#### Author details

<sup>1</sup>State Key Laboratory of Desert and Oasis Ecology, Xinjiang Institute of Ecology and Geography, Chinese Academy of Sciences, Urumqi, 830011, People's Republic of China. <sup>2</sup>Department of Geography, Hong Kong Baptist University, Kowloon Tong, Kowloon, Hong Kong, People's Republic of China. <sup>3</sup>Xinjiang University, Urumqi, 830046, People's Republic of China.

#### Acknowledgements

We thank the anonymous reviewers and the editor, whose comments and suggestions have helped improve the clarity of this manuscript. This work was supported by the National Natural Science Foundation of P.R. China (11401569, 11271312, 11361059), the Western Scholars of the Chinese Academy of Sciences (grant no. 2015-XBQN-B-20), and Natural Science Foundation of Xinjiang (2014211B047). And this work was also supported by the Hong Kong Scholars Program.

Received: 21 December 2015 Accepted: 25 May 2016 Published online: 13 June 2016

#### References

1. Zhou, L, Fan, M: Dynamics of an SIR epidemic model with limited medical resources revisited. *Nonlinear Anal., Real World Appl.* **13**, 312-324 (2012)
2. Alexanderian, A, Gobbert, MK, Fister, KR, Gaff, H, Lenhart, S, Schaefer, E: An age-structured model for the spread of epidemic cholera: analysis and simulation. *Nonlinear Anal., Real World Appl.* **12**, 3483-3498 (2011)

3. Zhang, H, Chen, L, Nieto, JJ: A delayed epidemic model with stage-structure and pulses for pest management strategy. *Nonlinear Anal., Real World Appl.* **9**, 1714-1726 (2008)
4. Robledo, G, Grognard, F, Gouzé, JL: Global stability for a model of competition in the chemostat with microbial inputs. *Nonlinear Anal., Real World Appl.* **13**, 582-598 (2012)
5. Mena-Lorca, J, Hethcote, HW: Dynamical models of infectious disease as regulations of population sizes. *J. Math. Biol.* **30**, 693-716 (1992)
6. Zhang, T, Teng, Z: Global behavior and permanence of SIRS epidemic model with time delay. *Nonlinear Anal., Real World Appl.* **9**, 1409-1424 (2008)
7. Wang, L, Chen, L, Nieto, JJ: The dynamics of an epidemic model for pest control with impulsive effect. *Nonlinear Anal., Real World Appl.* **11**, 1374-1386 (2010)
8. Gao, S, Liu, Y, Nieto, JJ, Andrade, H: Seasonality and mixed vaccination strategy in an epidemic model with vertical transmission. *Math. Comput. Simul.* **81**, 1855-1868 (2011)
9. McCluskey, CC: Complete global stability for an SIR epidemic model with delay-distributed or discrete. *Nonlinear Anal., Real World Appl.* **11**, 55-59 (2010)
10. Muroya, Y, Enatsu, Y, Nakata, Y: Monotone iterative technique to SIRS epidemic models with nonlinear incidence rates and distributed delays. *Nonlinear Anal., Real World Appl.* **12**, 1897-1910 (2011)
11. D'Innocenzo, A, Paladini, F, Renna, L: A numerical investigation of discrete oscillating epidemic models. *Physica A* **364**, 497-512 (2006)
12. Willox, R, Grammaticos, B, Carstea, AS, Ramani, A: Epidemic dynamics: discrete-time and cellular automaton models. *Physica A* **328**, 13-22 (2003)
13. Allen, LJS, Driessche, P: The basic reproduction number in some discrete-time epidemic models. *J. Differ. Equ. Appl.* **14**, 1127-1147 (2008)
14. Li, X, Wang, W: A discrete epidemic model with stage structure. *Chaos Solitons Fractals* **26**, 947-958 (2005)
15. Li, L, Sun, G, Jin, Z: Bifurcation and chaos in an epidemic model with nonlinear incidence rates. *Appl. Math. Comput.* **216**, 1226-1234 (2010)
16. Allen, LJS: Some discrete-time SI, SIR, and SIS epidemic models. *Math. Biosci.* **124**, 83-105 (1994)
17. Allen, LJS, Lou, Y, Nevai, AL: Spatial patterns in a discrete-time SIS patch model. *J. Math. Biol.* **58**, 339-375 (2009)
18. Franke, JE, Yakubu, A-A: Discrete-time SIS epidemic model in a seasonal environment. *SIAM J. Appl. Math.* **66**, 1563-1587 (2006)
19. Mendez, V, Fort, J: Dynamical evolution of discrete epidemic models. *Physica A* **284**, 309-317 (2000)
20. Sekiguchi, M: Permanence of a discrete SIRS epidemic model with time delays. *Appl. Math. Lett.* **23**, 1280-1285 (2010)
21. Muroya, Y, Bellen, A, Enatsu, Y, Nakata, Y: Global stability for a discrete epidemic model for disease with immunity and latency spreading in a heterogeneous host population. *Nonlinear Anal., Real World Appl.* **13**, 258-274 (2012)
22. Muroya, Y, Nakata, Y, Izzo, G, Vecchio, A: Permanence and global stability of a class of discrete epidemic models. *Nonlinear Anal., Real World Appl.* **12**, 2105-2117 (2011)
23. Franke, JE, Yakubu, A-A: Disease-induced mortality in density-dependent discrete-time S-I-S epidemic models. *J. Math. Biol.* **57**, 755-790 (2008)
24. Castillo-Chavez, C, Yakubu, A-A: Discrete-time SIS models with complex dynamics. *Nonlinear Anal.* **47**, 4753-4762 (2001)
25. Li, J, Ma, Z, Brauer, F: Global analysis of discrete-time SI and SIS epidemic models. *Math. Biosci. Eng.* **4**, 699-710 (2007)
26. Satsuma, J, Willox, R, Ramani, A, Grammaticos, B, Carstea, AS: Extending the SIR epidemic model. *Physica A* **336**, 369-375 (2004)
27. Sekiguchi, M, Ishiwata, E: Global dynamics of a discretized SIRS epidemic model with time delay. *J. Math. Anal. Appl.* **371**, 195-202 (2010)
28. Allen, LJS, Burgin, AM: Comparison of deterministic and stochastic SIS and SIR models in discrete time. *Math. Biosci.* **163**, 1-33 (2000)
29. Emmert, KE, Allen, LJS: Population extinction in deterministic and stochastic discrete-time epidemic models with periodic coefficients with applications to amphibian populations. *Nat. Resour. Model.* **19**, 117-164 (2006)
30. Li, J, Lou, J, Lou, M: Some discrete SI and SIS epidemic models. *Appl. Math. Mech.* **29**, 113-119 (2008)
31. Ramani, A, Carstea, AS, Willox, R, Grammaticos, B: Oscillating epidemics: a discrete-time model. *Physica A* **333**, 278-292 (2004)
32. Zhang, D, Shi, B: Oscillation and global asymptotic stability in a discrete epidemic model. *J. Math. Anal. Appl.* **278**, 194-202 (2003)
33. Hu, Z, Teng, Z, Jiang, H: Stability analysis in a class of discrete SIRS epidemic models. *Nonlinear Anal., Real World Appl.* **13**, 2017-2033 (2012)
34. Mena-Lorca, J, Hethcote, HW: Dynamical models of infectious disease as regulations of population sizes. *J. Math. Biol.* **30**, 693-716 (1992)
35. Hu, Z, Teng, Z: Permanence and extinction analyses of a discrete SIRS epidemic model. *Acta Math. Appl. Sin.* **37**, 547-556 (2014)
36. Guckenheimer, J, Holmes, P: *Nonlinear Oscillations, Dynamical Model and Bifurcation of Vector Field*, pp. 160-165. Springer, New York (1983)
37. Wang, L, Teng, Z, Jiang, H: Global attractivity of a discrete SIRS epidemic model with standard incidence rate. *Math. Methods Appl. Sci.* **36**, 601-619 (2013)
38. Hu, Z, Teng, Z, Jia, C, Zhang, L, Chen, X: Complex dynamical behaviors in a discrete eco-epidemiological model with disease in prey. *Adv. Differ. Equ.* **2014**, 265 (2014)
39. Yi, N, Zhang, Q, Liu, P, Lin, Y: Codimension-two bifurcations analysis and tracking control on a discrete epidemic model. *J. Syst. Sci. Complex.* **24**, 1033-1056 (2011)
40. Chen, Q, Teng, Z, Wang, L: The existence of codimension-two bifurcation in a discrete SIS epidemic model with standard incidence. *Nonlinear Dyn.* **71**, 55-73 (2013)